LLC converter with Reconfigurable Voltage Multiplier Rectifier for High Voltage and Wide Output Range Applications

Ming Shang, *Student Member, IEEE*, and Haoyu Wang, *Member, IEEE*
School of Information Science and Technology
ShanghaiTech University, Shanghai, China, 201210
Email: wanghy@shanghaitech.edu.cn

***Abstract*—In wide output applications, the switching frequency of conventional LLC converter needs to swing in a wide range, which jeopardizes the conversion efficiency. Moreover, the high output voltage brings high voltage stresses to the secondary side diodes. To cope with those issues, a novel LLC topology with reconfigurable voltage multiplier rectifier is proposed. This converter is suitable for both high output voltage and wide output range applications. Its rectifier may switch between voltage quadrupler and sixfolder configurations, depending on the desired output voltage. Benefits include narrow switching frequency range, low circulating current, and reduced conduction loss. Zero-voltage-switching (ZVS) and zero-current-switching (ZCS) are realized among all power MOSFETs and all power diodes, respectively. The voltage stresses on secondary side diodes are constrained. Detailed circuit operation principles and modeling method are presented. A 1.3 kW converter prototype, generating 500 V- 840 V output from 390 V dc link is designed and tested. Both the circuit functionality and the theoretical analysis are verified by the experimental results.**

Keywords—LLC; voltage quadrupler; voltage sixfolder; wide output voltage; ZVS; ZCS

I. INTRODUCTION

Nowadays, LLC resonant converter is one of the prevalent isolated dc/dc topologies due to its attractive features: a) ZVS among all the primary side MOSFETs; b) ZCS among all the secondary side diodes; c) wide output voltage range tuned by frequency modulation; and d) full ZVS range over the entire load range [1], [2]. Thus, it is widely used in applications where both a wide output voltage range and galvanic isolation are required [3]–[5].

Plug-in electric vehicle (PEV) onboard charging is such a typical application [6]. Its output must be matched with the voltage of the onboard battery pack, whose typical voltage range is between 250 V and 420 V [7]–[9]. In recent years, both the trends of electric mileage extension and the rapid increase of auxiliary power require an increase in the capacity of the PEV onboard battery [10]. Therefore, more battery cells need to be placed in series to enhance the battery capacity and endurance. This directly leads to an increase of the battery pack terminal voltage [11]. Moreover, in applications of electric buses or heavy-duty electric trucks, a battery pack voltage of 500 V - 840 V is desired.

However, deploying LLC resonant topology with full bridge rectifier in high voltage and wide output range applications has its nature limitations [12]. This is mainly due to two facts. On one hand, the voltage ratings of the bridge rectifier diodes are high and equal to the output voltage. This brings challenges to the diodes selection and may jeopardize the system reliability. On the other hand, LLC converter is a frequency modulated topology. This means its switching frequency (f_s) must swing in a wide range to fit this wide voltage gain range. This phenomenon can be observed clearly from the gain-frequency curves of the LLC topology, as plotted in Fig. 1. This makes f_s deviate from the resonant frequency (f_r). Thus, the conversion efficiency degrades fast.

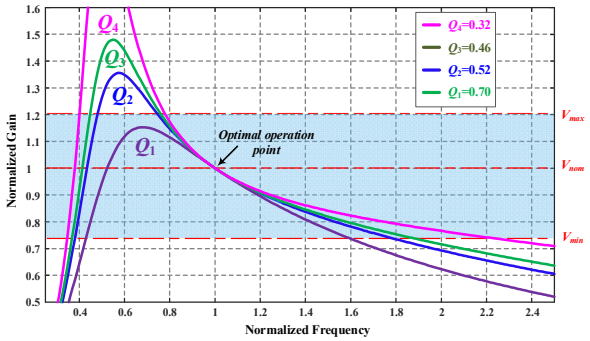

Fig. 1. DC voltage characteristics of LLC topology adapted to wide output voltage range.

To cope with the voltage stress of full bridge rectifier, the typical solution is to introduce a voltage multiplier rectifier to lower down the voltage stresses. Normally, those rectifiers include different configurations, such as voltage doubler rectifier, voltage tripler rectifier, voltage quadrupler rectifier, etc[13]–[15]. The other techniques to boost the voltage gain of LLC topology have also been explored in the literature. In [16], an interleaved boost-integrated LLC resonant converter is proposed. With the interleaved structure, the proposed converter can acquire a high voltage gain. However, this topology is designed for wide input voltage range applications and more suitable for photovoltaic systems. In [17], a current-fed boost converter and LLC resonant converter are cascaded for fuel cell systems. However, the boost stage operates in a hard-switching manner. This constrains its efficiency performance in high switching frequency.

To make the LLC converter suitable for the wide gain range, many modified LLC type converters are proposed [18]–[21].Two PWM LLC resonant topologies are reported in [18], [19]. In [18], a center-tapped transformer and a full wave rectifier are adopted. However, this topology is more suitable

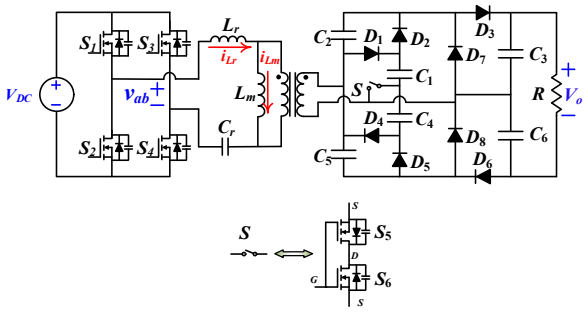

Fig. 2. Schematic of the proposed converter.

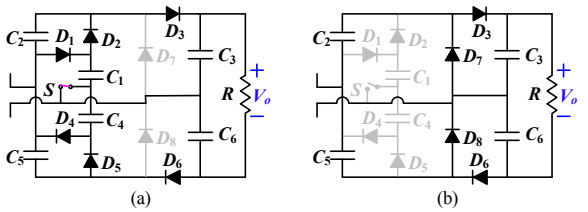

Fig. 3. Converter equivalent circuits: (a) *S* is ON, (b) *S* is OFF.

for wide input applications. In [19], the converter is mainly designed for light load applications. Similar to [18], the topology proposed in [20] is mainly investigated in wide input range applications. In high output voltage applications, it is not an optimal candidate with a full bridge rectifier. In [21], phase shift control is introduced on the secondary side to extend the voltage gain. However, it is mainly designed to compensate the switching frequency deviation in the short hold-up mode.

In this paper, a novel LLC converter with variable-structure voltage multiplier rectifier is proposed. This proposed converter achieves a wide output range with small f_s range. The charging voltage and current are regulated by modulating f_s with actively controlling the four quadrant switch on the secondary side. The proposed converter demonstrates benefits including a) ZVS turning on of all active switches, b) ZCS turning off of all diodes, c) reduced components voltage stresses on the second side, and e) reduced circulating current and conduction losses.

II. Proposed Converter

A. Topology Description

The schematic of the proposed converter is plotted in Fig. 2. The primary side of this topology is identical to that of the full bridge LLC resonant converter. All the MOSFETs have a constant duty cycle close to 0.5. The secondary side is composed of eight diodes, six capacitors, and a four quadrant switch (S). This structure is derived from the conventional voltage quadrupler rectifier (VQR) and the voltage sixfolder rectifier (VSR). As shown, *S* is composed of two series connected MOSFETs. They are turned on and off simultaneously.

B. Operation Principle

In the proposed converter, the primary side full bridge generates a two-level (V_{DC}, $-V_{DC}$) square waveform at the switching frequency. When *S* is always ON, the circuit

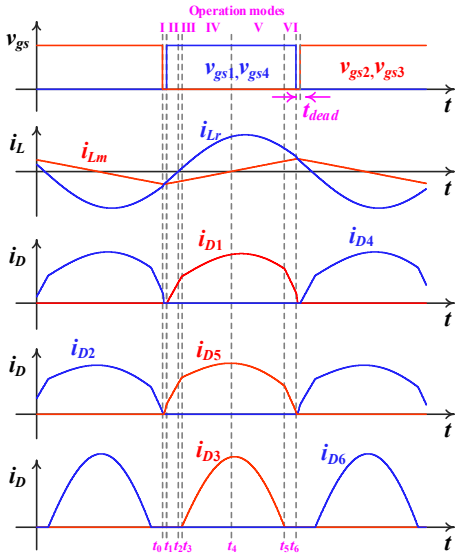

Fig. 4. Steady state waveforms in VSR mode.

operates in VSR configuration as shown in Fig. 3(a). When *S* is always OFF, the circuit operates in VQR configuration as shown in Fig. 3(b). In comparison with VQR and SVR structures, this circuit reconfiguration enables a much wider output voltage range.

In either configuration, the output is regulated by frequency modulation of the primary side full bridge. The switching frequency f_s can be greater, equal and less than the resonant frequency f_r. Only the waveforms of $f_s = f_r$ are analyzed and plotted Fig. 4.

1) VSR Configuration: The key steady state waveforms in VSR configuration are plotted in Fig. 4. The operation principle is similar to that of the conventional LLC resonant converter. To prevent shoot through, the upper and lower power MOSFETs are turned on and off complementarily with certain deadband (t_{dead}). In each switching cycle, there are 12 different operating modes. The two adjacent half switching periods are symmetrical. One half switching period, [t_0, t_6), is extracted for detail analysis. Those operating modes correspond to 6 equivalent circuits and are plotted in Fig. 5.

The operating modes analysis is based on the assumption that $C_{1\text{-}6}$ are sufficiently large, such that their voltage ripples can be ignored. Thus, those capacitors are modeled as dc voltage sources, $V_{1\text{-}6}$, respectively.

Mode I: [t_0, t_1). At $t_{0\text{-}}$, S_1 and S_4 are ON, L_r resonates with C_r. At t_0, S_1 and S_4 are turned off. The resonant current (i_{Lr}) is negative. Thus, the output parasitic capacitors of S_1 and S_4 are discharged to zero and then the corresponding body diodes conduct. This creates a zero voltage condition for the turning on of the MOSFETs.

Mode II: [t_1, t_2). At t_1, S_2 and S_3 are turned on with ZVS. The voltage across L_m is nV_1. As shown in Fig. 5, D_1 and D_5 start to conduct. Mode II ends when i_{Lr} reaches zero.

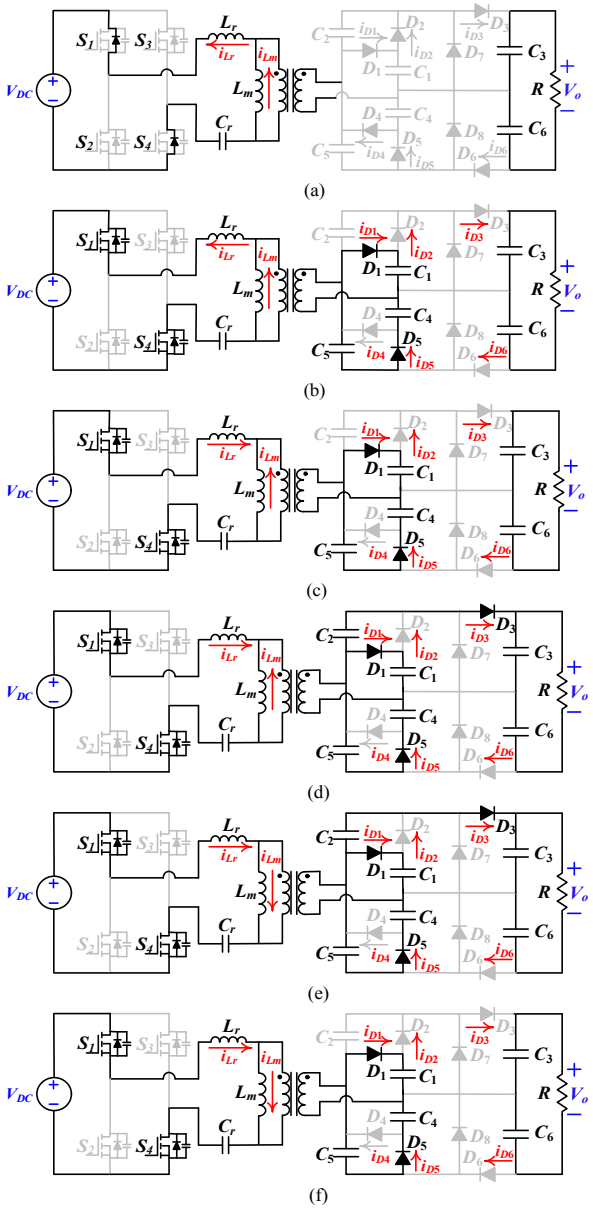

Fig. 5. Breakdown of operation modes.

Mode III: [t_2, t_3). Mode III begins at t_2 when i_{Lr} changes to be positive. L_r continues to resonate with C_r. The secondary current keeps flowing through D_1 and D_5.

Mode IV [t_3, t_4). At t_3, D_3 begins to conduct, the magnetizing inductor current (i_{Lm}) continues to increase linearly.

Mode V: [t_4, t_5). Mode V begins at t_4 when i_{Lm} reaches zero. In this mode, i_{Lm} changes to be positive. On the secondary side, the circuit operation is the same as the previous mode.

Mode VI: [t_5, t_6). At t_5, the current through D_3 (i_{D3}) reaches zero. In this mode, D_3 is turned off with zero current. Mode VI ends when i_{Lm} intersects with i_{Lr}.

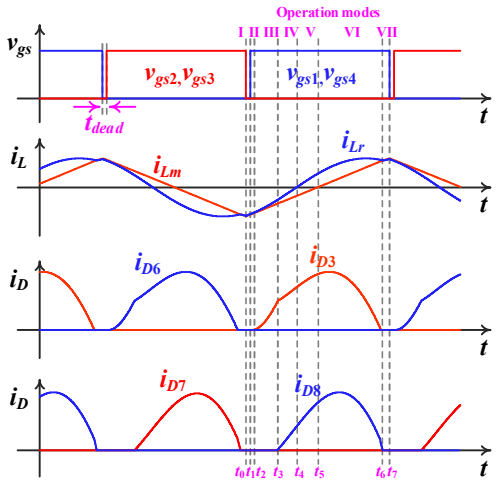

Fig. 6. Steady state waveforms in VQR mode.

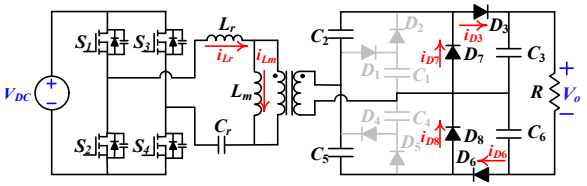

Fig. 7. Converter equivalent circuit in VQR mode.

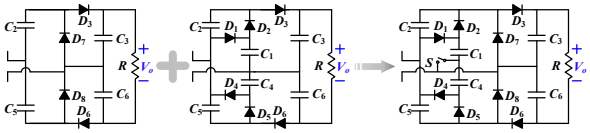

Fig. 8. Topology derivation. (a) Symmetrical VQR circuit. (b) Symmetrical VSR circuit. (c) Proposed converter.

Due to the circuit symmetry, the next mode is similar to mode I. ZCS of $D_{1,5}$ is guaranteed.

2) VQR Configuration: The key steady state waveforms in VQR configuration are plotted in Fig. 6. In comparison with VSR configuration, the main difference is that S is always OFF. This means $D_{1,2,4,5}$ are always off. Thus C_1 and C_4 are inactive. The equivalent circuit is plotted in Fig.7.

In this configuration, the operation principle is similar to that of VSR configuration. All the MOSFETs are turned on with ZVS. All the diodes are turned off with ZCS. The principles of the VQR converter structure has been analyzed in [22].

III. Characteristics and Analysis

A. Topology Derivation and Comparison

Fig. 8 shows the deviation process of this topology. We come to this topology by merging a conventional symmetrical voltage quadrupler rectifier and a symmetrical voltage sixfolder rectifier. This merge is facilitated by adding a four quadrant switch. This novel VSR rectifier is proposed by simply extending the VQR rectifier. In VQR configuration, the output voltage is four times of the amplitude of the transformer

TABLE I
VOLTAGES STRESS AND DC GAIN OF VARIOUS LLC RESONANT CONVERTERS

Secondary side circuit	*Voltage stress of diode*	*Voltage stress of capacitor*	*Maximum Gain*
Full wave rectifier	$2V_o$	V_o	M
Full bridge rectifier	V_o	V_o	M
Voltage quadrupler rectifier	$V_o/2$	$V_o/2, V_o/4$	4M
Voltage sixfolder rectifier	$V_o/3$	$V_o/2, V_o/3, V_o/6$	6M

secondary side voltage. This means $V_o = 2V_3 = 4V_2$. Similarly, in VSR configuration, the output voltage is six times of the amplitude of the transformer secondary side voltage. This means $V_o = 2V_3 = 3V_2 = 6V_1$.

The voltage stresses and maximum gain of the LLC converter with different secondary side rectifiers are compared. The results are listed in Table I. Since the proposed converter is derived from VQR and VSR configuration, it inherits the advantages of both converters. Those advantages include a) the lowest diode voltage stress, b) highest voltage gain and c) reduced transformer secondary side turns number. Therefore, a compact transformer and low voltage rating diodes can be selected. This helps to improve the performances of both the system power density and conversion efficiency.

B. Output Voltage Range Enhancement

The equivalent circuit in VSR configuration is plotted in Fig. 3(a). In this configuration, the voltage balance for C_3 and C_6 can be easily achieved. Therefore, the voltages across C_3 or C_6 are equal to the half of the output voltage. Meanwhile, the voltage across C_1 is half of the voltage across C_2, and the sum of the voltages across C_1 and C_2 also equals to the voltage across C_3. Thus, in this configuration, the output voltage (when $f_s = f_r$) is defined as,

$$V_o = \frac{6V_{DC}}{n} \tag{1}$$

The circuit operation is similar to that in the VSR configuration. All the MOSFETs and diodes can achieve ZVS turn on and ZCS turn off, respectively. Meanwhile, the voltages across C_3 and C_6 are equal to half of the output voltage. The sum of the voltages across C_5 and C_2 also equals to half of the output voltage. The output voltage (when $f_s = f_r$) is defined as,

$$V_o = \frac{4V_{DC}}{n} \tag{2}$$

Fig. 9 plots the voltage gain curves of the proposed topology in VQR configuration and VSR configuration based on the first harmonic approximation (FHA) approach. As shown, using the frequency modulation, the output voltage range using this reconfigurable structure can be further

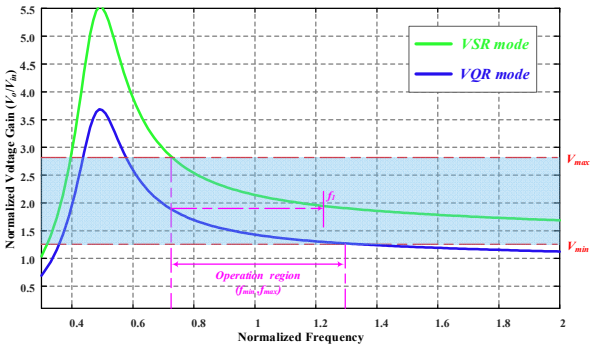

Fig. 9. Normalized voltage gain versus normalized frequency.

extended. This means an extremely wide output voltage range (V_{min}, V_{max}) can be achieved with a narrow switching frequency range (f_{min}, f_{max}). As shown in Fig. 9, the maximum output voltage (in VQR) should be larger than the minimum output voltage (in VSR) to make sure the output voltage is continuous in full output range. This means f_{max} should be larger than f_1.

C. Design Considerations

In LLC type resonant topologies, f_r, Q and L_n are the resonant frequency, quality factor, and inductance ratio between L_m and L_r, respectively.

$$f_r = \frac{1}{2\pi\sqrt{L_r C_r}} \tag{3}$$

$$L_n = \frac{L_m}{L_r} \tag{4}$$

$$Q = \frac{\sqrt{L_r / C_r}}{n^2 R} \tag{5}$$

where, R is the equivalent load resistance; f_r, Q, and L_n can be designed based on the FHA method. The detailed analysis has been discussed comprehensively in [23].

It should be noted that there exists a secondary resonance in the LLC resonant tank. This resonance happens when L_m participles into the resonance between L_r and C_r. Thus, this resonance frequency f_m is the resonance frequency between (L_r + L_m) and C_r,

$$f_m = \frac{1}{2\pi\sqrt{(L_r + L_m)C_r}} \tag{6}$$

The switching frequency is designed to be larger than f_m. This enables that the resonant tank works in the inductive region with ZVS feature.

First, we need to justify the output threshold voltage. Below this voltage, the converter operates in VQR configuration. Above this voltage, the converter operates in VSR configuration. Then, we need to optimally design each individual configuration based on the corresponding load conditions. This design process is similar to that of the conventional LLC converter. Special attention must be paid to

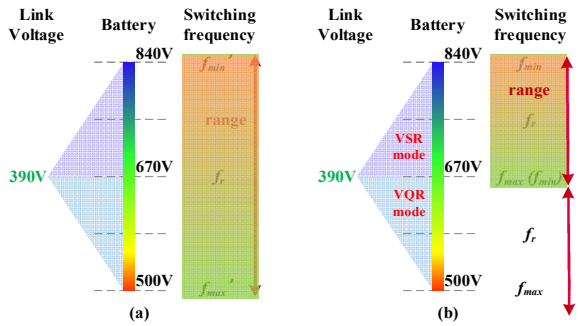

Fig. 10. Output voltage and switching frequency range for fixed DC-link voltage (390V): a) conventional converter; b) proposed converter.

the voltage gain and the switching frequency range. This can be observed from Fig. 10. The components parameters need to suitable for both VSR and VQR converter.

IV. Experimental Results

TABLE II
Circuit Specifications and Design Parameters

Symbol	Quantity	Parameter
V_i	Input voltage	390 V
V_o	Output voltage	500 V – 840 V
L_r	Resonant inductor	57 μH
C_r	Resonant capacitor	44 nF
L_m	Magnetizing inductor	260 μH
$C_{1\text{-}6}$	Output capacitor	150 μF
n	Transformer turns ratio	2.6
f_s	Switching frequency	100 kHz
D	Diode	RHRG30120
$S_{1,2,3,4}$	Primary side MOSFET	IRFP460
$S_{5,6}$	Secondary side MOSFET	88N65M5

To verify the effectiveness of the proposed converter, a 390 V input, 500 V – 840 V output, 1.3 kW, 100 kHz converter prototype is designed and tested. The specifications and design parameters are summarized in Table II.

The steady-state waveforms of the proposed LLC converter in VQR configuration with V_o = 633 V are captured in Fig. 11. It can be seen that v_{ds1} and v_{ds2} drop to zero before gate signals are applied to the MOSFETs. Therefore, ZVS is achieved on both S_1 and S_2. At this operating point, the waveforms of i_{D6} and i_{D7} show the zero current turning off of the secondary diodes.

Fig. 12 demonstrates the operations of the converter at VSR configuration with output voltage equals to 810 V. The waveform of i_{Lr} shows that the converter works in the vicinity of f_r. As shown, v_{ds1} is discharged to zero before the gate signal is applied to S_1. Therefore, S_1 is turned on with ZVS. Fig. 12(b) mainly demonstrates the ZCS turning off of the secondary diodes. Figures 11 and 12 both verify the steady-state waveforms agree with the analysis in Section II-B pretty well.

Fig. 13 shows the curves of efficiency versus output voltage with constant output current 1.5 A. At 650 V output voltage, VSR configuration demonstrates slightly higher efficiency than VQR configuration. Therefore, 650 V is selected as the threshold voltage to trigger the configuration switch. When the

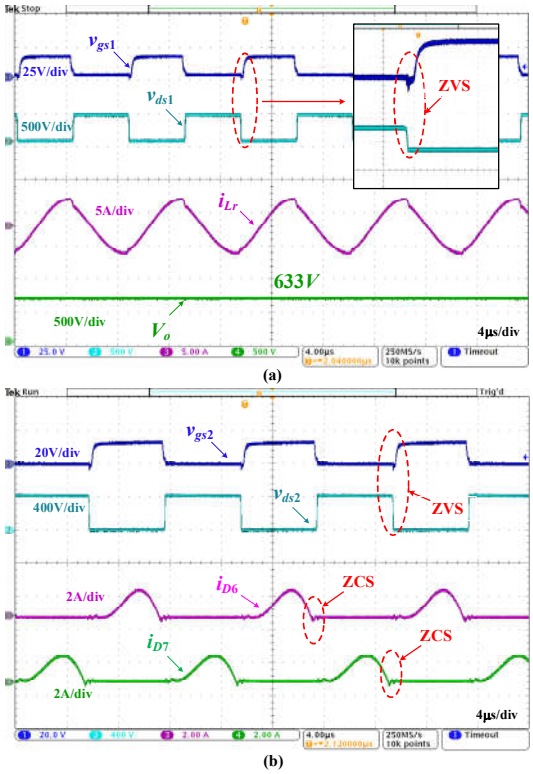

Fig. 11. Steady state waveforms in VQR mode: a) the ZVS realization of S_1 with V_o = 633 V; b) the ZVS and ZCS realization.

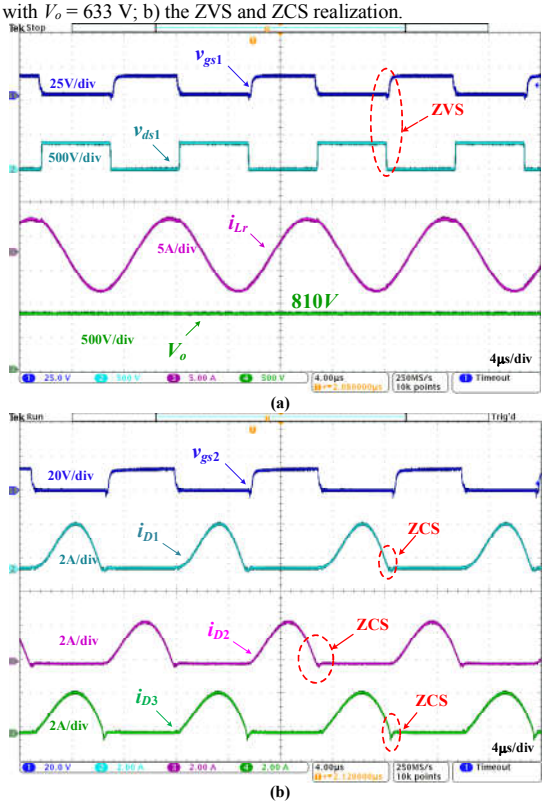

Fig. 12. Steady state waveforms in VSR mode: a) the ZVS realization of S_1 with V_o = 810 V; b) the ZCS realization.

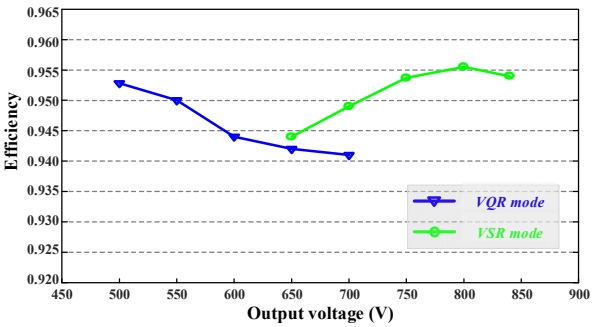

Fig. 13. Measured converter efficiency versus output voltages with I_o =1.5 A.

output voltage is below 650V, the converter operates in VDR configuration. The conversion efficiency slightly degrades with the increase of the output voltage. With output voltage above 650 V, the converter operates in VSR configuration. The conversion efficiency increase with the increase of the output voltage and reaches the peak value (95.5%) at 800 V output. This prototype demonstrates overall good efficiency over a wide output voltage.

V. Conclusions

In this paper, a novel self-reconfigurable LLC type resonant topology is proposed for use in high voltage and wide output range applications. The circuit operation principles are analyzed. The advantages of the proposed converter are detailed. The converter can operate with a small switching frequency range by dynamically changing the operation configuration of the rectifier. ZVS and ZCS are realized among all power MOSFETs and all power diodes. In comparison with conventional LLC resonant converter with a full bridge rectifier, the proposed converter is more suitable for wide output range and high output voltage applications. A 1.3 kW converter prototype is designed to verify the proof of concept. The proposed topology is not only useful for PEV battery charging applications but also worth pursuing in applications where a wide voltage gain range is desired.

Acknowledgement

This work was supported in part by the National Natural Science Foundation of China under Grant 51607113, and in part by the Shanghai Sailing Program under Grant 16YF1407600

References

[1] Z. Guo, D. Sha, and X. Liao, "Hybrid Phase-Shift-Controlled Three-Level and LLC DC – DC Converter With Active Connection at the Secondary Side," *IEEE Trans. Power Electron.*, vol. 30, no. 6, pp. 2985–2996, 2015.

[2] H. Wang, S. Dusmez, and A. Khaligh, "Maximum Efficiency Point Tracking Technique for LLC-Based PEV Chargers Through Variable DC Link Control," *IEEE Trans. Ind. Electron.*, vol. 61, no. 11, pp. 6041–6049, Nov. 2014.

[3] H. Wu, X. Zhan, and Y. Xing, "Interleaved LLC Resonant Converter With Hybrid Rectifier and Variable-Frequency Plus Phase-Shift Control for Wide Output Voltage Range Applications," *IEEE Trans. Power Electron.*, vol. 32, no. 6, pp. 4246–4257, Jun. 2017.

[4] H. Wang, S. Dusmez, and A. Khaligh, "Design and Analysis of a Full-Bridge LLC-Based PEV Charger Optimized for Wide Battery Voltage Range," *IEEE Trans. Veh. Technol.*, vol. 63, no. 4, pp. 1603–1613, May 2014.

[5] F. Musavi, M. Craciun, D. S. Gautam, W. Eberle, and W. G. Dunford, "An LLC Resonant DC–DC Converter for Wide Output Voltage Range Battery Charging Applications," *IEEE Trans. Power Electron.*, vol. 28, no. 12, pp. 5437–5445, Dec. 2013.

[6] J. Lee and H. Chae, "6 . 6-kW Onboard Charger Design Using DCM PFC Converter With Harmonic Modulation Technique and Two-Stage DC / DC Converter," *IEEE Trans. Ind. Electron.*, vol. 61, no. 3, pp. 1243–1252, 2014.

[7] H. Wang, "A phase shift full bridge based reconfigurable PEV onboard charger with extended ZVS range and zero duty cycle loss," in *2016 IEEE Applied Power Electronics Conference and Exposition (APEC)*, 2016, pp. 480–486.

[8] I.-O. Lee, "Hybrid PWM-Resonant Converter for Electric Vehicle On-Board Battery Chargers," *IEEE Trans. Power Electron.*, vol. 31, no. 5, pp. 3639–3649, May 2016.

[9] H. Wang, M. Shang, and A. Khaligh, "A PSFB-Based Integrated PEV Onboard Charger With Extended ZVS Range and Zero Duty Cycle Loss," *IEEE Trans. Ind. Appl.*, vol. 53, no. 1, pp. 585–595, Jan. 2017.

[10] G.-J. Su and L. Tang, "A new integrated onboard charger and accessory power converter for plug-in electric vehicles," in *2014 IEEE Energy Conversion Congress and Exposition (ECCE)*, 2014, pp. 4790–4796.

[11] C. Botsford and A. Szczepanek, "Fast Charging vs . Slow Charging : Pros and cons for the New Age of Electric Vehicles," in *24th Electric Vehicle Symposium*, 2009, no. May, pp. 1–9.

[12] Z. Fang, T. Cai, S. Duan, and C. Chen, "Optimal Design Methodology for LLC Resonant Converter in Battery Charging Applications Based on Time-Weighted Average Efficiency," *IEEE Trans. Power Electron.*, vol. 30, no. 10, pp. 5469–5483, 2015.

[13] N. A. Samsudin, S. Iqbal, and S. Taib, "LLC resonant high-voltage DC-DC converter with voltage multiplier rectifier," in *2015 IEEE International Conference on Control System, Computing and Engineering (ICCSCE)*, 2015, pp. 508–513.

[14] O. Converters, Y. Zhao, S. Member, X. Xiang, W. Li, and X. He, "Advanced Symmetrical Voltage Quadrupler Rectifiers for High Step-Up and High," vol. 28, no. 4, pp. 1622–1631, 2013.

[15] P. Lin and L. Chua, "Topological generation and analysis of voltage multiplier circuits," *IEEE Trans. Circuits Syst.*, vol. 24, no. 10, pp. 517–530, Oct. 1977.

[16] X. Sun, Y. Shen, Y. Zhu, and X. Guo, "Interleaved Boost Integrated LLC Resonant Converter With Fixed-Frequency PWM Control for Renewable Energy Generation Applications," *IEEE Trans. Power Electron.*, vol. 8993, no. c, pp. 4312–4326, 2014.

[17] J.-Y. Lee, Y.-S. Jeong, and B.-M. Han, "An Isolated DC/DC Converter Using High-Frequency Unregulated LLC Resonant Converter for Fuel Cell Applications," *IEEE Trans. Ind. Electron.*, vol. 58, no. 7, pp. 2926–2934, Jul. 2011.

[18] X. Sun, X. Li, Y. Shen, B. Wang, and X. Guo, "Dual-Bridge LLC Resonant Converter with Fixed-Frequency PWM Control for Wide Input Applications," *IEEE Trans. Power Electron.*, vol. 32, no. 1, pp. 69–80, 2017.

[19] F. Ajmal, H. Pan, C. He, G. Chen, and H. Chen, "Pulse-width modulation control strategy for high efficiency LLC resonant converter with light load applications," *IET Power Electron.*, vol. 7, no. 11, pp. 2887–2894, Nov. 2014.

[20] I. H. Cho, Y. Do Kim, and G. W. Moon, "A half-bridge llc resonant converter adopting boost PWM control scheme for hold-up state operation," *IEEE Trans. Power Electron.*, vol. 29, no. 2, pp. 841–850, 2014.

[21] H. Wu, T. Mu, X. Gao, and Y. Xing, "A Secondary-Side Phase-Shift-Controlled LLC Resonant Converter With Reduced Conduction Loss at Normal Operation for Hold-Up Time Compensation Application," *IEEE Trans. Power Electron.*, vol. 30, no. 10, pp. 5352–5357, Oct. 2015.

[22] Y. Zhao, X. Xiang, W. Li, X. He, and C. Xia, "Advanced Symmetrical Voltage Quadrupler Rectifiers for High Step-Up and High Output-

Voltage Converters," *IEEE Trans. Power Electron.*, vol. 28, no. 4, pp. 1622–1631, Apr. 2013.

[23] C. Y. Hsu, J. T. Lai, M. C. Lin, M. K. Yang, M. J. Li, and R. W. Huang, "The design and implementation of LLC resonant half-bridge converter with natural interleaved power-factor-correction," *Proc. Int. Conf. Power Electron. Drive Syst.*, no. December, pp. 246–255, 2011.